THE JOURNAL OF PHYSICAL CHEMISTRY C

ARTICLE

pubs.acs.org/JPCC

Porous Fe_3O_4/Carbon Core/Shell Nanorods: Synthesis and Electromagnetic Properties

Yu-Jin Chen,*[,†] Gang Xiao,[†] Tie-Shi Wang,[†] Qiu-Yun Ouyang,[†] Li-Hong Qi,[†] Yang Ma,[†] Peng Gao,*[,‡] Chun-Ling Zhu,*[,‡] Mao-Sheng Cao,[§] and Hai-Bo Jin[§]

[†]College of Science and [‡]College of Material Science and Chemical Engineering, Harbin Engineering University, Harbin 15001, China

[§]School of Materials Science and Engineering, Beijing Institute of Technology, Beijing 100081, China

Supporting Information

ABSTRACT: The porous Fe_3O_4/carbon core/shell nanorods were fabricated via a three-step process. α-Fe_2O_3 nanorods were first obtained, and α-Fe_2O_3/carbon core/shell nanorods were subsequently fabricated using glucose as a carbon source by a hydrothermal method, in which the thickness of the carbon coating was about 3.5 nm. Fe_3O_4/carbon core/shell nanorods were synthesized after an annealing treatment of the product above under a mixture of Ar/H_2 flow. After the H_2 deoxidation process, the Fe_3O_4 core exhibited a character of porosity; the thickness of the carbon shell was decreased to about 2.5 nm, and its degree of graphitization was enhanced. The interesting core/shell nanostructures are ferromagnetic at room temperature, and the Verwey temperature was about 120 K. Electromagnetic properties of the core/shell nanorod−wax composite were investigated in detail. The maximum reflection loss was about −27.9 dB at 14.96 GHz for the composite with a thickness of 2.0 mm, and the absorption bandwidth with the reflection loss below −18 dB was up to 10.5 GHz for the absorber with the thickness of 2−5 mm. The excellent electromagnetic wave absorption properties of the porous Fe_3O_4/carbon core/shell nanorods were attributed to effective complementarities between the dielectric loss and the magnetic loss.

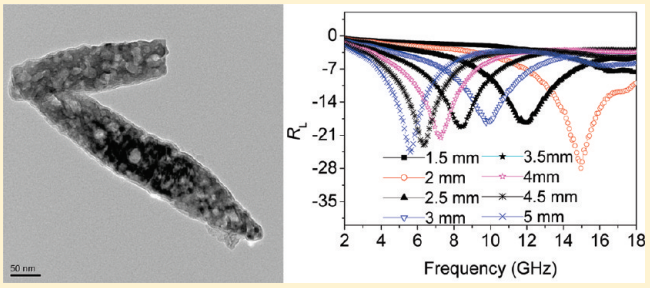

1. INTRODUCTION

Fe_3O_4 is a kind of important magnetic material and has attracted physical properties such as half-metallic character and strong spin polarization at room temperature. Its magnetic properties can be tuned by the size, shape, and dimensions.[1−3] Thus, Fe_3O_4 has wide applications in many areas such as gas sensors, optoelectronic and spintronic devices, Li ion battery, and biomedicine, etc.[1−3] However, uncoated Fe_3O_4 nanostructures would be limited in some application areas, and thus several strategies were developed to synthesize multifunctional Fe_3O_4-based nanocomposites.[4] Previous researches mainly focused on zero-dimensional nanocomposites. For example, nano-Ru/Fe_3O_4 hybrids were prepared and used as catalysts for the synthesis of sulfonamides.[4a] Au, Ag, or polymer-coated Fe_3O_4 nanoparaticles were fabricated for biolabeling or bioimaging.[4b−e] Silica/magnetite nanocomposite was synthesized for magnetic bioseparations.[4f] Wang et al. recently fabricated Fe_3O_4/ZnS hollow nanospheres by the corrosion-aided Ostwald ripening process and found that the nanocomposite exhibited superparamagnetic and fluorescent properties.[4g] Recently, it has been found that one-dimensional (1 D) Fe_3O_4 nanocomposites also exhibit improved chemical and physical properties.[5] Daly et al. synthesized 1 D Co/Fe_3O_4 nanocable arrays by the anodic aluminum oxide template method and found that the nanocomposite exhibited ferro- and ferrimagnetic properties at room temperature with the saturation magnetization up to 20% lower than expected for the bulk material.[5b] 1 D Fe_3O_4 nanocomposites such as carbon-decorated Fe_3O_4 nanowires have been used to improve their electrochemical performances.[5c−e] The reports above demonstrate that the configuration of the core/shell nanostructures can extend to material applications.

Recently, many nanostructures have been developed to attenuate electromagnetic (EM) wave because the thickness of the traditional absorbers is required to be too large.[6−10] Among those nanostructures, core/shell nanostructures have been exhibited very good EM absorption properties due to the interfacial polarization, confinement effect, and effective complementarities between the dielectric loss and the magnetic loss. For example, the reflection loss can be up to more than −25 dB for carbon nanotube/Fe nanocomposite with the thickness of only 1.2 mm.[10a] Therefore, core/shell nanostructures may be used as new types of the absorbers for the attenuation of EM wave. Here we developed a three-step process to fabricate interesting Fe_3O_4/carbon core/shell nanorods with ferromagnetic characteristics at

Received: March 15, 2011
Revised: May 9, 2011
Published: June 23, 2011

room temperature. The Fe_3O_4 core has many pores along its axis, and the carbon shell has enhanced degree of graphitization. Especially, effective complementarities between the dielectric loss and the magnetic loss enable the porous core/shell nanorods to attenuate electromagnetic wave at the frequency region over 2−18 GHz.

2. EXPERIMENTAL SECTION

Porous Fe_3O_4/carbon core−shell nanorods were fabricated through a three-step process. (1) α-Fe_2O_3 nanorods were first obtained by the modified method reported by Jia and co-workers.[11] Simply, specific amounts of $FeCl_3$ and $NH_4H_2PO_4$ were added into 40 mL of water under vigorous stirring; the concentrations of $FeCl_3$ and $NH_4H_2PO_4$ in the final mixture were 0.02 and 7.15×10^{-4}, respectively. The mixture was then transferred into a Teflon-lined stainless steel autoclave with a capacity of 50 mL for hydrothermal treatment at 220 °C for 4 h. As the autoclave cooled to room temperature naturally, the precipitates were separated by centrifugation, washed with distilled water and absolute ethanol, and dried in air. (2) α-Fe_2O_3/carbon nanorods were fabricated by a wet-chemical method. Typically, 0.1 g of α-Fe_2O_3 nanorods was dispersed in 32 mL of water−alcohol solvent by ultrasonication. Then 0.6 g of glucose was put into the solution above. The mixture was then transferred into a Teflon-lined stainless steel autoclave with a capacity of 50 mL for hydrothermal treatment at 190 °C for 12 h. After reaction, the autoclave was cooled naturally in air, and the suspensions were isolated by filtration, washed with water and absolute ethanol several times, and dried in oven at 60 °C for 12 h under vacuum. (3) The product obtained above was treated at 360 °C for 6 h under a mixture of Ar/H_2 flow. After the annealing treatment, the porous Fe_3O_4/carbon core/shell nanorods were obtained by the above processes.

The morphology and the size of the synthesized samples were characterized by scanning electron microscopy (SEM) [JEOL-JSM-6700F] and transmission electron microscope (TEM) [JEOL 2010]. The crystal structure of the sample was determined by X-ray diffraction (XRD)[D/max 2550 V, Cu Kα radiation], X-ray photoelectron spectroscopy (XPS) [PHI 5300 ESCA, Al Kα radiation], and Raman spectroscopy (λ_{exc}, 532 nm).

Surface properties of the porous core/shell nanorods were studied by the Brunauer−Emmett−Teller (BET) methods via nitrogen adsorption and desorption measurements. The magnetic properties were measured by a superconducting quantum interference device (SQUID) magnetometer and a vibrating sample magnetometer (VSM).

The composite sample used for EM absorption measurement was prepared by mixing porous Fe_3O_4/carbon core/shell nanorods with wax with a weight ratio of 55%. The mixture was then pressed into toroidal-shaped samples (φ_{out}: 7.00 mm; φ_{in}: 3.04 mm). The complex permittivity and permeability of the composite were measured by using the T/R coaxial line method. The measurement setup consisted of an HP 8722ES vector network analyzer with a synthesized sweep oscillator source and an *S*-parameter test set.

3. RESULTS AND DISCUSSION

Figure 1a is a typical XRD pattern of as-synthesized α-Fe_2O_3/carbon nanorods. Compared with the data in JCPDS No. 33-0664, all peaks indicated by Miller indices in the pattern can be

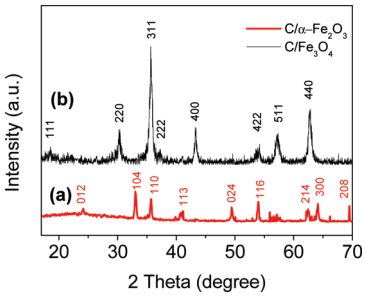

Figure 1. XRD patterns of (a) α-Fe_2O_3/carbon core/shell nanorods and (b) Fe_3O_4/carbon core/shell nanorods.

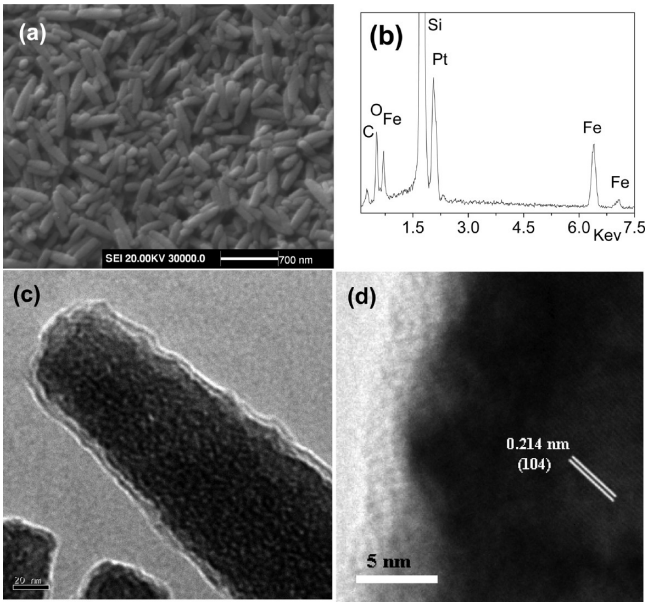

Figure 2. Structural characterizations of α-Fe_2O_3/carbon core/shell nanorods: (a) A SEM image, (b) EDS spectrum, (c) TEM, and (d) HRTEM images.

indexed to α-Fe_2O_3. It suggests that α-Fe_2O_3 nanorods are still highly crystalline after the carbon coating. In the pattern, except the diffraction peaks from α-Fe_2O_3, no other ones are obviously observed, suggesting an amorphous character of the carbon shell.

Figure 2a shows a typical SEM image of α-Fe_2O_3/carbon core/shell nanorods. It can be seen that the surface of the nanocomposite is very smooth, and the average length and the diameter of the core/shell nanorods are about 80 and 390 nm, respectively. The carbon coating is not clearly observed in the SEM image, but the peaks of O, Fe, and C elements are presented in the energy dispersive spectroscopy (EDS) spectrum (Figure 2b), indicating that the nanocomposite contains carbon component. The TEM image (Figure 2c) reveals that the surface of α-Fe_2O_3 nanorods was fully covered with a thin carbon film, and the overall thickness of the film is about 3.5 nm. Figure 2b shows a high-resolution (HR) TEM image of the core/shell nanorods. The *d*-spacing of the core is 0.214 nm, corresponding to (101) lattice plane of α-Fe_2O_3 nanorods. No crystalline lattice is observed in the outer layer. It indicates that the carbon coating is highly disordered, which is consistent with the XRD result.

XRD, EDS, and TEM analyses demonstrate that α-Fe_2O_3/carbon core/shell nanorods are fabricated in the present method.

dx.doi.org/10.1021/jp202473y |*J. Phys. Chem. C* 2011, 115, 13603–13608

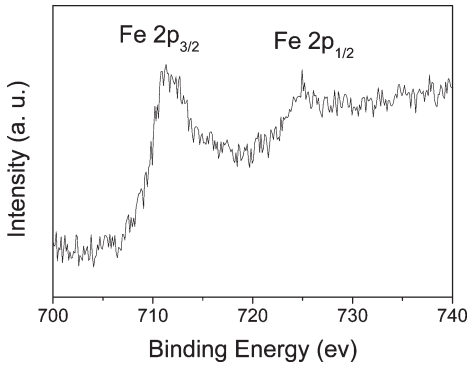

Figure 3. Fe 2p core level XPS spectrum for the Fe_3O_4/carbon core/shell nanorods.

After the annealing treatment under a Ar/H_2 flow, the structures of the nanocomposite were largely changed. Figure 1b shows the XRD pattern of the product obtained after the annealing treatment, in which all diffraction peaks indicated by Miller indices in the pattern can be indexed to cubic Fe_3O_4 structures (JPCDS card number 72-2303). This implies that α-Fe_2O_3 in the nanocomposite may be transformed into Fe_3O_4. However, because of the very similar patterns between γ-Fe_2O_3 and Fe_3O_4, the XRD analyses cannot provide enough evidence to confirm the transformation. XPS spectroscopy can be used to determine the difference in the oxidation state of the iron. Figure 3 shows Fe 2p core level XPS spectrum of the Fe_3O_4/carbon core/shell nanorods. Two main peaks, located at 711.3 and 724.9 eV, correspond to Fe $2p_{3/2}$ and Fe $2p_{1/2}$, respectively. The signals are broadened, indicating that the Fe^{3+} and Fe^{2+} states coexisted in the core/shell nanorods. Moreover, no shakeup satellite peaks, which are the fingerprints of the electronic structures of iron oxides such as α-Fe_2O_3 and γ-Fe_2O_3, can be identified. It indicates that Fe_2O_3 is not presented in the core/shell nanorods.[12] In addition, the color of the final product was changed into black, which also supports the result above.

The structure of Fe_3O_4/carbon core/shell nanorods was further characterized by TEM observation. One-dimensional morphology of the nanorods was still well preserved due to the presence of carbon layer on the surface of the nanorods, as shown in Figure 4a. Furthermore, the Fe_3O_4 core has many pores along the axis direction. The magnified TEM image (Figure 4b) shows the diameter of the pores is in range of 4−28 nm. The porous property of the Fe_3O_4/carbon core/shell nanorods was further investigated by the BET methods via nitrogen adsorption and desorption measurement. Figure 5 shows the nitrogen adsorption−desorption isotherms of the nanocomposite. From the figure, the BET surface area of the core/shell nanorods is 45.2 m^2/g. The inset in Figure 5 is the corresponding pore size distribution of the nanocomposite calculated from the desorption branch of N_2 isotherm. The pore size distributions is mainly in range of 5−27 nm, and the mean pore diameter is about 12 nm, which is consistent with the TEM observations.

From the TEM image, it can be also found that the surface of the core is still fully covered with a thin carbon layer. HRTEM images (Figure 4c,d) show the overall thickness of the carbon coating is about 2.5 nm. It reveals that the thickness of the carbon is decreased after the H_2 deoxidation process. The decrease may result from the weight loss of the absorption of a small quantity of water and the graphitization of the outer carbon layer. The degree of

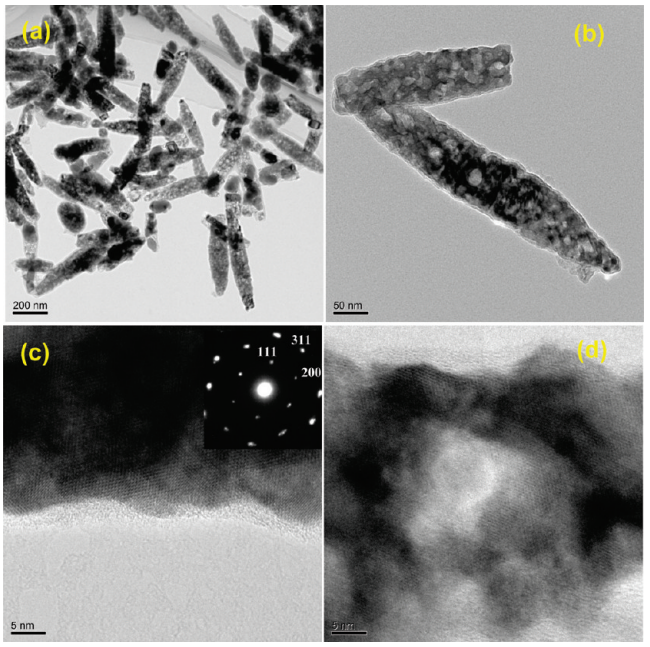

Figure 4. Structural characterizations of porous Fe_3O_4/carbon core/shell nanorods: (a) a low-resolution TME image, (b) a magnified TEM image, (c) and (d) HRTEM images. The inset in (c) shows the SAED pattern.

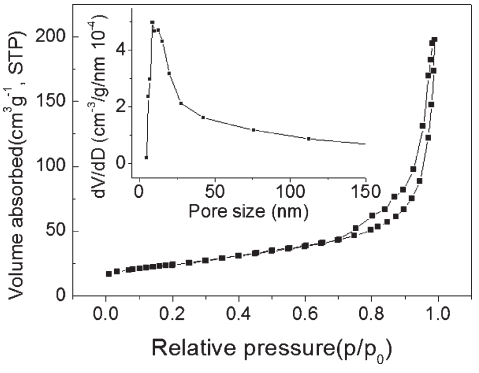

Figure 5. Nitrogen adsorption−desorption isotherms of porous Fe_3O_4/carbon core/shell nanorods. Inset: the BJH pore-size distribution of the nanocomposite calculated from the desorption branch of N_2 isotherm.

graphitization of the carbon in α-Fe_2O_3 and Fe_3O_4 nanocomposites was investigated by Raman spectroscopy, and the results are shown in Figure 6. All sample spectra show two peaks about 1380 and 1594 cm^{-1}. The Raman-active E_{2g} mode at 1594 cm^{-1} (G-bands) is characteristic for graphitic sheets, whereas the D-band at around 1380 cm^{-1} can be attributed to the presence of sp^3 defects within the carbon.[13] Thus, the intensity ratio of the D- and G-band ($I_{D\text{-band}}/I_{G\text{-band}}$) is indicative of the degree of graphitization. The ratio value for Fe_3O_4/carbon core/shell nanorods is 0.7724, whereas it is 0.8125 for α-Fe_2O_3/carbon core/shell nanorods. This indicates that the degree of graphitization of the carbon within Fe_3O_4 nanocomposite is strongly enhanced.

The temperature-dependent magnetic properties of the Fe_3O_4/carbon core/shell nanorods were investigated using the SQUID technique. Figure 7a shows the field-cooled (FC) and zero-field-cooled (ZFC) magnetization (M) versus temperature

dx.doi.org/10.1021/jp202473y |J. Phys. Chem. C 2011, 115, 13603–13608

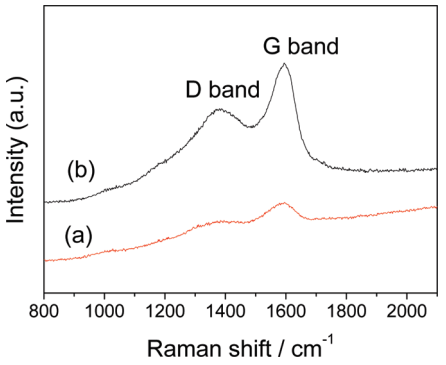

Figure 6. Raman shifts of (a) α-Fe_2O_3/carbon core/shell nanorods and (b) Fe_3O_4/carbon core/shell nanorods.

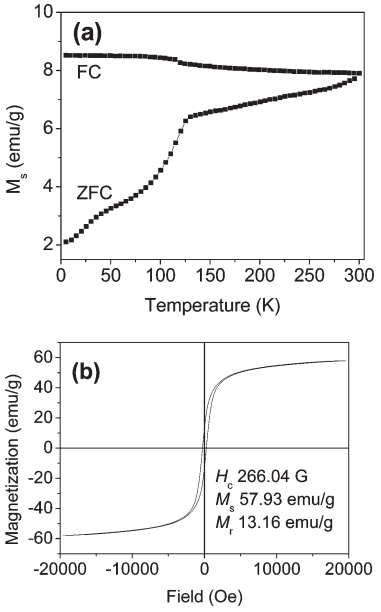

Figure 7. (a) FC and ZFC curves of porous Fe_3O_4/carbon core/shell nanorods with an applied external field of 300 Oe. (b) Magnetization hysteresis loops of porous Fe_3O_4/carbon core/shell nanorods measured at room temperature.

curves under an applied external field (H) of 300 Oe. An apparent magnetic transition around 120 K is observed in the ZFC curve, which corresponds to the Verwey transition.[14] It arises from a fast electron hopping process between Fe^{3+} and Fe^{2+} ions. The Verwey transition temperature (T_v) is about 120 K, implying that the structure transition can result in a change of the electrical and magnetic properties at above the temperature.[15] The field dependence of magnetization for Fe_3O_4/carbon core/shell nanorods was also measured by VSM at room temperature, as shown in Figure 7b. Significant hysteresis loops in the $M-H$ curve indicate the ferromagnetic behavior of the core/shell nanorods. The saturation magnetization (M_s), coercivity (H_c), and retentivity (M_r) are 57.93 emu/g, 266.04 Oe, and 13.16 emu/g, respectively. The value of M_s is smaller than the corresponding bulk value (92 emu/g)[16] and bare Fe_3O_4 nanorods which was obtained through the annealing treatment of α-Fe_2O_3 nanorods at 360 °C for 6 h under a mixture of Ar/H_2 flow (Figure S1). The decrease in the magnitization is attributed to the nonmagnetic carbon coating.

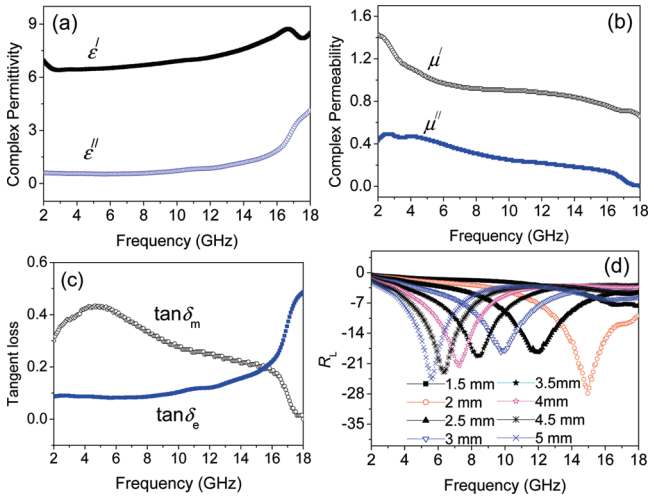

Figure 8. (a) Complex permittivity, (b) the complex permeability, (c) the tangent loss, and (d) the reflection loss of porous Fe_3O_4/carbon core/shell nanorods.

Ferromagnetic Fe_3O_4/carbon core/shell nanorods were fabricated by the present method. The nanocomposite exhibits some interesting characters: (1) the dense interface is presented between the core and shell regions; (2) there are many pores along the Fe_3O_4 axis; (3) the carbon coating has enhanced degree of graphitization. Furthermore, both carbon and Fe_3O_4 materials have exhibited electromagnetic (EM) response.[6] Thus, the porous Fe_3O_4/carbon core/shell nanorods are expected to show strong EM absorption properties. The electromagnetic parameters (relative complex permittivity, $\varepsilon_r = \varepsilon' - j\varepsilon''$ and relative complex permeability, $\mu_r = \mu'_r - j\mu''_r$) of the wax composite containing 55 wt % of the porous Fe_3O_4/carbon core/shell nanorods were measured at room temperature for the investigation of EM absorption properties. Figure 8a shows the frequency dependence of the relative complex permittivity of the porous Fe_3O_4/carbon core/shell nanorods. The ε' and ε'' values are in the range of 6.4−8.73 and 0.53−4.14 at frequency region over 2−18 GHz, respectively. Those values, especially for imaginary parts, are higher than or comparable to those of ZnO-coated Fe nanocapsules,[7] Fe_3O_4/TiO_2 core/shell nanotubes,[5g] and ZnO nanowires.[8] It suggests that Fe_3O_4/carbon core/shell nanorods have strong dielectric loss against EM wave. The dielectric tangent loss ($\tan\delta_e = \varepsilon''/\varepsilon'$) of the porous Fe_3O_4/carbon core/shell nanorods is shown in Figure 8c. The $\tan\delta_e$ values larger than 0.2 are distributed from 15.6 to 18 GHz, indicating that the dielectric loss occurs at the high-frequency range. In terms of the electromagnetic theory such high dielectric loss is resulted from the naturally physical properties of Fe_3O_4 and the special core/shell structures. The diploes present in Fe_3O_4 especially when their sizes are in nanoscale.[5g,h] The number of surface atoms with unsaturated bonds would greatly increase as the size decreases, resulting in an increase of the dipoles. Consequently, the dipole polarizations can contribute to the dielectric loss. The dielectric loss is also related to electron hopping between Fe^{2+} and Fe^{3+} ions as the EM wave applied at the temperature above T_v (Figure 7a).[17] Furthermore, the interfacial polarization and the associated relaxation occurred at the interfaces between the core and the shell also contribute to the dielectric loss.[9] In addition, according to the free-electron theory, $\varepsilon'' = 1/2\pi\varepsilon_0\rho f$, where ρ is the resistivity. The resistivity of

the nanocomposite will decrease due to the enhanced degree of graphitization of the carbon coating and results in the increase of the dielectric loss.

The complex permeability for the core/shell nanorod−wax composite (Figure 8b) indicates that the μ' value is in the range of 0.66−1.43, and the μ'' value is larger than 0.1 at the frequency region of 2−16.64 GHz. The μ'' value is significantly larger with respect to other EM absorption materials, e.g., ZnO-coated iron nanoparticles,[9d] carbon-coated Ni nanocapsules,[9j] and Fe_3O_4/TiO_2 core/shell nanostructures.[5f] Especially, the μ'' value first increases, and then it decreases slightly and exhibits a broadened resonance peak with a maximum value of 0.49 at 2−6 GHz. According to the natural-resonance equation[18]

$$2\pi f_r = rH_a \quad (1)$$

$$H_a = 4|K_1|/3\mu_0 M_S \quad (2)$$

where r is the gyromagnetic ratio, H_a is the anisotropy energy, and $|K_1|$ is the anisotropy coefficient. The r value is 2.8 GHz/kOe, and the K_1 for bulk Fe_3O_4 is about -9×10^{-3} J m^{-3}; thus, the resonance frequency should be around 1.5 GHz. That resonance shift to high frequency is attributed to the small size effect.[18] It is believed that the anisotropy energy of small size materials, especially on nanometer scale, would be remarkably increased due to the surface anisotropic field by the small size effect.[19] In addition, Fe_3O_4 confined within the carbon with some degree graphitization is expected to be influenced by its local environment of confinement by an effective anisotropy field.[10] Such high-frequency resonance loss is important for EM wave absorption. From the data in Figure 8b, the magnetic tangent loss ($\tan \delta_m = \mu'/\mu''$) was calculated, and the result is shown in Figure 8c. The $\tan \delta_m$ values higher than 0.2 are at the frequency region over 2−15.4 GHz, indicating that the magnetic loss plays the main role in the EM absorption at the low-frequency range. In general, the EM wave absorptions are strongly dependent on the efficient complementarities between the dielectric loss and the magnetic loss. Only the dielectric loss or magnetic loss leads to weak EM attenuation. The porous Fe_3O_4/carbon core/shell nanorods fabricated in the present work show strong dielectric loss at the high-frequency range and significant magnetic loss at the low-frequency range. Such complementarities between the dielectric loss and the magnetic loss imply that the porous core/shell nanorods have excellent EM absorption properties.

On the basis of the transmit-line theory,[20] the reflection loss (R_L) can be calculated by the equations

$$Z_{in} = (\mu_r/\varepsilon_r)^{1/2} \tanh[j2\pi fd/c)(\mu_r\varepsilon_r)^{1/2}] \quad (3)$$

$$R_L\ (dB) = 20 \log \left|\frac{Z_{in} - 1}{Z_{in} + 1}\right| \quad (4)$$

where Z_{in} is the input impedance of the absorber, μ_r and ε_r are respectively the relative complex permeability and permittivity, c is the velocity of electromagnetic waves in free space, f is the frequency of microwaves, and d is the thickness of the absorber. The reflection loss of the core/shell nanorods with the sample thickness varied from 2 to 5 mm can be calculated, and the results are shown in Figure 8d. It indicates that the maximum reflection loss reaches −27.9 dB at 14.96 GHz for the absorber whose thickness is 2 mm. Moreover, the absorption bandwidth with the reflection loss below −18 dB is up to 10.5 GHz (from 5.2 to 15.7 GHz) for the absorber with the thickness in 2−5 mm. Since the absorber with the R_L values less than −10 dB can be designed to attenuate EM wave, thus the core/shell nanorods are very promising for new types of EM wave absorptive materials. In addition, for the comparison of the EM absorption properties of Fe_3O_4/carbon nanocomposite with bare Fe_3O_4 nanorods, we also calculated the reflection loss of Fe_3O_4/wax composite with the same weight addition as Fe_3O_4/carbon nanocomposite, and the result is shown in Figure S2a. The reflection loss of Fe_3O_4/wax composite is less than −10 dB as its thickness varied from 2 to 5 mm. It is largely less than that of Fe_3O_4/carbon core/shell nanorods, which is attributed to that the dielectric loss of the bare Fe_3O_4 nanorods is significantly higher than it is the magnetic loss (Figure S2b).

4. CONCLUSIONS

In summary, ferromagnetic Fe_3O_4/carbon core/shell nanorods with the Verwey temperature of about 120 K have been fabricated by the present method. The Fe_3O_4 core has many pores whose mean diameter is about 12 nm, and the shell exhibits an enhanced degree of graphitization. The interesting core/shell nanostructures exhibit high magnetic loss at the low-frequency range and strong dielectric loss at the high-frequency range. Combined the complementarities with special core/shell structures, porous characters and graphitic carbon coating, the core/shell nanorods can be used as EM wave absorber.

■ ASSOCIATED CONTENT

Supporting Information. Magnetic and electromagnetic properties of bare Fe_3O_4 nanorods. This material is available free of charge via the Internet at http://pubs.acs.org.

■ AUTHOR INFORMATION

Corresponding Author

*E-mail: chenyujin@hrbeu.edu.cn (Y.-J.C.), gaopeng@hrbeu.edu.cn (P.G.), and zhuchunling@hrbeu.edu.cn (C.-L.Z.).

■ ACKNOWLEDGMENT

The authors acknowledge the support from the National Natural Science Foundation of China (Grants 51072038 and 21001035), NECT, Outstanding Youth Foundation of Heilongjiang Province (Grant JC201008), Natural Science Foundation of Heilongjiang Province, China (Grants F200828 and E200839), Project supported by the Ministry of Science and Technology of China (Grant 2008DFR20420), the Fundamental Research Funds for the Central Universities (Grants HEUCFT1010, HEUCF20111127, HEUCF20111124, and HEUCF101016), and also Harbin Key Sci-tech Project (Grant 2010AA4BG004).

■ REFERENCES

(1) (a) Huh, Y. M.; Jun, Y. W.; Song, H. T.; Kim, S. J.; Choi, J. S.; Lee, J. H.; Yoon, S.; Kim, K. S.; Shin, J. S.; Suh, J. S.; Cheon, J. *J. Am. Chem. Soc.* **2005**, *127*, 12387. (b) Lee, H.; Lee, E.; Kim, D. K.; Jang, N. K.; Jeong, Y. Y.; Jon, S. *J. Am. Chem. Soc.* **2006**, *128*, 7383. (c) Wang, X.; Zhuang, J.; Peng, Q.; Li, Y. D. *Nature* **2005**, *437*, 121. (d) Peng, S.; Sun, S. H. *Angew. Chem., Int. Ed.* **2007**, *46*, 4155. (e) Kim, D.; Lee, N.; Park, M.; Kim, B. H.; An, K.; Hyeon, T. *J. Am. Chem. Soc.* **2009**, *131*, 454.

(f) Liu, Z. Q.; Zhang, D. H.; Han, S.; Li, C.; Lei, B.; Lu, W. G.; Fang, J. Y.; Zhou, C. W. *J. Am. Chem. Soc.* **2005**, *127*, 6.

(2) (a) Tang, J. K.; Wang, K. Y.; Zhou, W. L. *J. Appl. Phys.* **2001**, *89*, 7690. (b) Gee, S. H.; Hong, Y. K.; Erickson, D. W.; Park, M. H.; Sur, J. C. *J. Appl. Phys.* **2003**, *93*, 7560. (c) Lu, Z. L.; Xu, M. X.; Zou, W. Q.; Wang, S.; Liu, X. C.; Lin, Y. B.; Xu, J. P.; Lu, Z. H.; Wang, J. F.; Lv, L. Y.; Zhang, F. M.; Du, Y. W. *Appl. Phys. Lett.* **2007**, *91*, 102508. (d) Venkatesan, M.; Nawka, S.; Pillai, S. C.; Coey, J. M. D. *J. Appl. Phys.* **2003**, *93*, 8023. (d) Goya, G. F.; Berquó, T. S.; Fonseca, F. C.; Morales, M. P. *J. Appl. Phys.* **2003**, *94*, 3520.

(3) (a) Hu, F. Q.; Wei, L.; Zhou, Z.; Ran, Y. L.; Li, Z.; Gao, M. Y. *Adv. Mater.* **2006**, *18*, 2553. (b) Mathur, S.; Barth, S.; Werner, U.; Hernadez-Ramirez, F.; Romano-rodriguez, A. *Adv. Mater.* **2008**, *20*, 1550. (c) Li, Z.; Tan, B.; Allix, M.; Cooper, A. I.; Rosseinsky, M. J. *Small* **2008**, *4*, 231. (d) Jun, Y. W.; Huh, Y. M.; Choi, J. S.; Lee, J. H.; Song, H. T.; Kim, S. J.; Yoon, S.; Kim, K. S.; Shin, J. S.; Suh, J. S.; Cheon, J. *J. Am. Chem. Soc.* **2005**, *127*, 5732. (e) Kim, M.; Chen, Y. F.; Liu, Y. C.; Peng, X. G. *Adv. Mater.* **2005**, *17*, 1429.

(4) (a) Shi, F.; Tse, M. K.; Zhou, S. L.; Pohl, M. M.; Radnik, J.; Hübner, S.; Jähnisch, K.; Brückner, A.; Beller, M. *J. Am. Chem. Soc.* **2009**, *131*, 1775. (b) Yu, H.; Chen, M.; Rice, P. M.; Wang, S. X.; White, R. L.; Sun, S. H. *Nano Lett.* **2005**, *5*, 379. (c) Miywaki, J.; Yudasaka, M.; Imai, H.; Yorimitsu, H.; Isobe, H.; Nakamura, E.; Iijima, S. *Adv. Mater.* **2006**, *18*, 1010. (d) Gu, H. W.; Yang, Z. M.; Gao, J. H.; Chang, C. K.; Xu, B. *J. Am. Chem. Soc.* **2005**, *127*, 34. (e) Gao, J. H.; Huang, P. B.; Zhang, B. Z.; Zhang, X. X.; Xu, B. *J. Am. Chem. Soc.* **2008**, *130*, 3710. (f) Sen, T.; Sebastianelli, A.; Bruce, L. J. *Am. Chem. Soc.* **2006**, *128*, 7130. (g) Wang, Z. X.; Wu, L. M.; Chen, M.; Zhou, S. X. *J. Am. Chem. Soc.* **2009**, *131*, 11276.

(5) (a) Zhou, G. G.; Wang, D. W.; Li, F.; Zhang, L. L.; Wu, Z. S.; Wen, L.; Lu, G. Q.; Cheng, H. M. *Chem. Mater.* **2010**, *22*, 5306. (b) Daly, B.; Arnold, D. C.; Kulkarni, J. S.; Kazakova, O.; Shaw, M. T.; Nikitenko, S.; Erts, D.; Morris, M. A.; Holmes, J. D. *Small* **2006**, *2*, 1299. (c) Zhang, W. M.; Wu, X. L.; Hu, J. S.; Guo, Y. G.; Wan, L. J. *Adv. Funct. Mater.* **2008**, *18*, 3941. (d) Liu, H.; Wang, G. X.; Wang, J. Z.; Wexler, D. *Electrochem. Commun.* **2008**, *10*, 1879. (e) Taberna, L.; Mitra, S.; Poizot, P.; Simon, P.; Tarascon, J. M. *Nature Mater.* **2006**, *5*, 567. (f) Chen, Y. J.; Zhang, F.; Zhao, G. G.; Fang, X. Y.; Jin, H. B.; Gao, P.; Zhu, C. L.; Cao, M. S.; Xiao, G. *J. Phys. Chem. C* **2010**, *114*, 9239. (g) Zhu, C. L.; Zhang, M. L.; Qiao, Y. J.; Xiao, G.; Zhang, F.; Chen, Y. J. *J. Phys. Chem. C* **2010**, *114*, 16229. (h) Chen, Y. J.; Gao, P.; Wang, R. X.; Zhu, C. L.; Wang, Li-Jiao; Cao, M. S.; Jin, H. B. *J. Phys. Chem. C* **2009**, *113*, 10061.

(6) (a) Liu, J. R.; Itoh, M.; Horikawa, T.; Machida, K. I. *J. Appl. Phys.* **2005**, *98*, 054305. (b) Walts, P. C. P.; Hsu, W. K.; Barnes, A.; Chambers, B. *Adv. Mater.* **2003**, *15*, 600. (c) Wadhawan, A.; Garrett, D.; Perez, J. M. *Appl. Phys. Lett.* **2003**, *83*, 2683. (d) Yang, Y. L.; Gupta, M. C. *Nano Lett.* **2005**, *5*, 2131.

(7) Liu, X. G.; Geng, D. Y.; Meng, H.; Shang, P. J.; Zhang, Z. D. *Appl. Phys. Lett.* **2008**, *92*, 173117.

(8) Chen, Y. J.; Cao, M. S.; Wang, T. H.; Wan, Q. *Appl. Phys. Lett.* **2004**, *84*, 3367.

(9) (a) Zhou, R. F.; Feng, H. T.; Chen, J. T.; Yan, D.; Feng, J. J.; Li, H. J.; Geng, B. S.; Cheng, S.; Xu, X. Y.; Yan, P. X. *J. Phys. Chem. C* **2008**, *112*, 11767. (b) Chen, Y. J.; Gao, P.; Zhu, C. L.; Wang, R. X.; Wang, L. J.; Cao, M. S.; Fang, X. Y. *J. Appl. Phys.* **2009**, *106*, 054303. (c) Liu, X. G.; Geng, D. Y.; Zhang, Z. D. *Appl. Phys. Lett.* **2008**, *92*, 243110. (d) Zhang, X. F.; Dong, X. L.; Huang, H.; Liu, Y. Y.; Wang, W. N.; Zhu, X. G.; Lv, B.; Lei, J. P.; Lee, C. G. *Appl. Phys. Lett.* **2006**, *89*, 053115. (e) Lee, C. C.; Chen, C. H. *Appl. Phys. Lett.* **2007**, *90*, 193102. (j) Liu, X. G.; Geng, D. Y.; Meng, H.; Shang, P. J.; Zhang, Z. D. *Appl. Phys. Lett.* **2008**, *92*, 173117.

(10) (a) Che, R. C.; Zhi, C. Y.; Liang, C. Y.; Zhou, X. G. *Appl. Phys. Lett.* **2006**, *88*, 033105. (b) Che, R. C.; Peng, L. M.; Duan, X. F.; Chen, Q.; Liang, X. L. *Adv. Mater.* **2004**, *16*, 401.

(11) Jia, C. H.; Sun, L. D.; Luo, F.; Han, X. D.; Heyderman, L. J.; Yan, C. H.; Zheng, K.; Zhang, Z.; Takano, M.; Hayashi, N.; Eltschka, M.; Kläui, M.; Rüdiger, U.; Kasama, T.; Cervera-Gontard, L.; Dunin-Borkowski, R. E.; Tzvetkov, G.; Raabe, J. *J. Am. Chem. Soc.* **2008**, *130*, 16968.

(12) Fujii, T.; de Groot, F. M. F.; Sawatzky, G. A.; Voogt, F. C.; Hibma, T.; Okada, K. *Phys. Rev. B* **1999**, *59*, 3195.

(13) (a) Eklund, P. C.; Holden, J. M.; Jishi, R. A. *Carbon* **1995**, *33*, 959. (b) Su, F. B.; Zhao, X. S.; Wang, Y.; Zeng, J. H.; Zhou, Z. C.; Lee, J. Y. *J. Phys. Chem. B* **2005**, *109*, 20200. (c) Zhang, L. W.; Fu, H. B.; Zhu, Y. F. *Adv. Funct. Mater.* **2008**, *18*, 2180. (d) Chen, C.; Cai, W.; Long, M.; Zhou, B.; Wu, Y.; Wu, D.; Feng, Y. *ACS Nano* **2010**, *4*, 6425. (e) Dresselhaus, M. S.; Jorio, A.; Hofmann, M.; Dresselhaus, G.; Saito, R. *Nano Lett.* **2010**, *10*, 751. (f) Zhang, W. X.; Cui, J. C.; Tao, C. A.; Wu, Y. G.; Li, Z. P.; Ma, L.; Wen, Y. Q.; Li, G. T. *Angew. Chem., Int. Ed.* **2009**, *48*, 5864. (g) Lu, J.; Yang, J. X.; Wang, J.; Lim, A.; Wang, S.; Loh, K. P. *ACS Nano* **2009**, *3*, 2367.

(14) Verwey, E. J. W. *Nature* **1939**, *144*, 327.

(15) Venkatesan, M.; Nawka, S.; Pillai, S. C.; Coey, J. M. D. *J. Appl. Phys.* **2003**, *93*, 8023.

(16) Smit, J.; Wijn, H. P. *Ferrie*; Wiley: New York, 1959; p 369.

(17) Walz, F. *J. Phys.: Condens. Matter* **2002**, *14*, R285.

(18) Kittel, C. *Phys. Rev.* **1948**, *73*, 155.

(19) Diandra, L. L.; Reuben, D. R. *Chem. Mater.* **1996**, *8*, 1770.

(20) Miles, P. A.; Westphal, W. B.; Von Hippel, A. *Rev. Mod. Phys.* **1957**, *29*, 279.